Macromolecules

Article

pubs.acs.org/Macromolecules

Scattering Studies on Poly(3,4-ethylenedioxythiophene)−Polystyrenesulfonate in the Presence of Ionic Liquids

Ryan J. Murphy,*[,†] Katie M. Weigandt,[‡] David Uhrig,[§] Ahmed Alsayed,[†] Chantal Badre,[†] Larry Hough,[†] and Murugappan Muthukumar[∥]

[†]Complex Assemblies of Soft Matter, CNRS-SOLVAY-PENN UMI 3254, Bristol, Pennsylvania 19007-3624, United States

[‡]National Institute of Standards and Technology, 100 Bureau Dr., Gaithersburg, Maryland 20899, United States

[§]Center for Nanophase Materials Sciences, Oak Ridge National Laboratory, Oak Ridge, Tennessee 37831 United States

[∥]Department of Polymer Science and Engineering, Silvio O. Conte National Center for Polymer Research, University of Massachusetts Amherst, Amherst, Massachusetts 01003-9263, United States

Supporting Information

ABSTRACT: The demand for lower cost and flexible electronics has driven industry to develop alternative transparent electrode (TE) materials to replace indium tin oxide (ITO). ITO is the benchmark TE on the market, but its high cost and low flexibility limit it for use in future technologies. Recent work has shown the combination of the conducting polymer poly(3,4-ethylenedioxythiophene)−polystyrenesulfonate (PEDOT:PSS) with the ionic liquid 1-ethyl-3-methylimidazolium tetracyanoborate (EMIM:TCB) is a viable ITO replacement. The work presented here investigates the nature of the interaction between PEDOT:PSS and EMIM:TCB in the solution state. A combination of scattering methods is used to illustrate a novel, multilength scale model of this system. At length scales larger than 300 nm PEODT:PSS adopts a microgel-like structure, and below ∼300 nm the system adopts an entangled polyelectrolyte mesh structure. As EMIM:TCB is added, the microgel interior adopts a more neutral polymer mesh structure as EMIM:TCB concentration is increased.

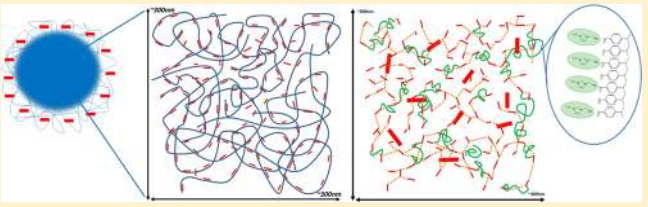

INTRODUCTION

Conducting polymers continue to garner significant excitement to enable the next-generation transparent conducting electrodes as alternatives to inorganic oxides. Among the latter class of materials, the benchmark material is indium tin oxide (In_2O_3:Sn, or ITO) which is a highly conductive metal oxide that is used as the transparent electrode (TE) in a wide range of devices such as touch screens, displays, and solar cells. ITO exhibits transparencies (T) of >98% and conductivities (S) of ∼1000−5000 S/cm. Despite its high performance, ITO has drawbacks large enough to drive the electronics industry to seek for alternatives; it is an expensive, brittle material that requires intensive processing, all of which combine to make it obsolete for use in lower cost electronics and next-generation flexible electronic devices. In order to enable these future technologies, conducting polymers have attracted significant efforts[1] as they satisfy the key parameters needed for next-generation transparent conducting electrodes. One of the more popular conducting polymers that has been investigated for this application is poly(3,4-ethylenedioxythiophene)−polystyrenesulfonate (PEDOT:PSS), shown in Figure 1a.

The PEDOT:PSS single chain structure is a polyelectrolyte chain (PSS) with oligomeric counterions (PEDOT) statistically associated along the PSS backbone,[2] as is illustrated in Figure 1b. PEDOT:PSS is an interesting fit for TE applications as it is conductive and water-soluble and has a work function value similar to ITO[3] which will not interfere with charge transport processes from adjacent material layers. Because of these properties, PEDOT:PSS is already used in various electronic devices as smoothing layers for ITO.[2] However, the main issue with using PEDOT:PSS as an ITO replacement is that it does not have a native conductivity high enough for this application. A host of work has gone into improving the conductivity of

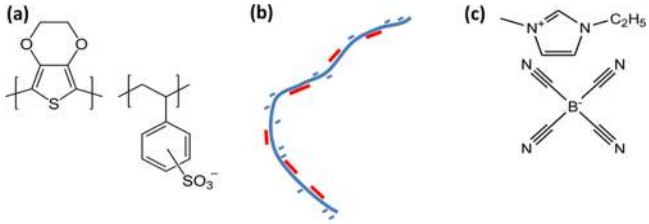

Figure 1. (a) Chemical structures of PEDOT:PSS, (b) single-chain structure of PEDOT:PSS, and (c) chemical structure of EMIM TCB. In (b), the blue chain represents the PSS while the red shorter chains represent the PEDOT oligomers associated with the PSS backbone. The negative charges illustrated in (b) are located in sites where the PSS chain is not conjugated with PEDOT.

Received: October 23, 2015
Revised: November 18, 2015
Published: November 30, 2015

DOI: 10.1021/acs.macromol.5b02320
Macromolecules 2015, 48, 8989−8997

PEDOT:PSS by adding organic solvents such as DMSO,[4−6] ethylene glycol,[7−10] DMF,[4] THF,[4] and various alcohols[9,11] as well as with ionic species such as metal salts,[12] surfactants,[13] and ionic liquids.[14−17] The latter additive has garnished particular interest due to their very low vapor pressure,[18] unique structural[19−24] and electrochemical[25−27] properties, versatile solubility profile,[28−30] and low toxicity.[31] Beyond conductivity improvement, ionic liquids have shown the ability to impart other functionality when combined with PEDOT:PSS, such as water resistance[15] and switchable wettability.[16] Recently, Badre et al.[32] showed that when PEDOT:PSS is combined with a specific ionic liquid, 1-ethyl 3-methylimidazolium tetracyanoborate (EMIM:TCB), the resulting films have conductivities of ∼2500 S/cm and transparencies of >98% in films that are <200 nm thick, making the PEDOT:PSS EMIM:TCB system a viable candidate for replacing ITO. The structure of EMIM:TCB is shown in Figure 1c.

This exciting result has clear commercial impact, but the morphological behaviors of PEDOT:PSS, water, and EMIM:TCB are complex, and understanding this system from a molecular perspective is crucial for harnessing its overall potential. There have been numerous studies focused on understanding the structure and performance enhancement mechanism of PEDOT:PSS in the solution[5,9] and film state[4,6−8,10−15,33−35] as a function of these various additives. To date, the mechanism of conductivity improvement in PEDOT:PSS films by these additives has been attributed to a combination of electrostatic screening of the PEDOT away from the PSS[4,12,13] and preferential solvation of PSS over PEDOT which promotes a phase separation into PSS-rich and PEDOT-rich domains.[6,8,11,33,34] Studies on the solution structure of PEDOT:PSS have generally concluded that the polymer takes on a nanometer size, micelle-like structure in water, with a PEDOT-rich core and PSS outer layer which provides the overall solubilization and stability of the polymer via electrostatic repulsion by uncompensated PSS monomers.[9] The addition of high-boiling-point solvent additives has been shown to promote expanded chain conformations of PEDOT:PSS in solution, which has been attributed to promoting better chain organization once the material is put into the film state.[5] However, there has been no comprehensive study on the solution structure of PEDOT:PSS with ionic liquid additives. Toward a better understanding of the system, the present work presents an investigation into the structure of the PEDOT:PSS water dispersion and how this structure changes upon addition of EMIM:TCB system. The approach of this study was to first understand each of the individual components of this system and subsequently studying the difference in their behavior once combined together. A novel, multilength scale structural model of PEDOT:PSS in water is proposed, and a mechanism that explains the change in PEDOT:PSS structure upon addition of EMIM:TCB is outlined.

EXPERIMENTAL SECTION

Materials. A highly conductive grade of poly(3,4-ethylenedioxythiophene) polystyrenesulfonate (PEDOT:PSS) was purchased from Clevios (PH1000) and used in this work.[a] Unless otherwise stated, the concentration of PEDOT:PSS in this work is ∼1.1 mass % in water, and the material was used as delivered. DMSO (ACS reagent ≥99.9%) was purchased from Sigma-Aldrich. 1-Ethyl 3-methylimidazolium tetracyanoborate (EMIM:TCB, ultrapure grade) was purchased from EMD Chemicals and used as received. For deuteration synthesis, styrene-d_8 was obtained from Cambridge Isotopes, and all other reagents were obtained from Sigma-Aldrich.

Synthesis of Deuterated Polystyrenesulfonate (DPSS). Perdeuterated polystyrene (dPSS, M_w ∼ 26 000 g/mol) was prepared at the Center for Nanophase Materials Sciences (CNMS) at Oak Ridge National Laboratory by polymerizing styrene-d_8 anionically.[36−38] This polymer was sulfonated with sulfur trioxide to obtain ≥83% sulfonated perdeuterated polystyrene (dPSS) by following the methods of Valint[39] and Yang.[40] This ionomer product was neutralized, dialyzed against neutral water, and reacidified with acidic ion-exchange resin to yield dPSS, in acid form, free of any excess acid or salt.

Synthesis of PEDOT:Deuterated-PSS (PEDOT:DPSS). PEDOT:deuterated-PSS, (PEDOT:dPSS) was then prepared by previously reported synthesis methods[41] and was also carried out at the Center for Nanophase Materials Sciences (CNMS) at Oak Ridge National Laboratory. In this case, the PSS product was replaced by the dPSS product described above, Briefly, 5.18 g of a 18% dPSS solution (5.06 mmol of monomer) was dissolved in 93 mL of deionized water. Then, 0.5 g (3.52 mmol) of EDOT was added, and the solution was tip sonicated for ∼1 min in order to have a milky solution. 0.9 g (3.33 mmol) of potassium persulfate and 95 μL (0.035 mmol) of a 10% $FeCl_3{\cdot}6H_2O$ solution were added to a glass bottle equipped with a mechanical stirrer and a nitrogen input. Polymerization of the EDOT was observed while stirring. The reactor was agitated very slowly for 24 h under nitrogen. The polymer was separated from the reaction medium by centrifuging (15 000 rpm for 30 min) and washed three times with water. Then 2.0 g of ion-exchange resin (J.T. Baker IONAC NM-60 H+/OH-Form, Type I, beads, 16−50 mesh) was added to the reactor, which was stirred for a day.

In order to test the product against the commercial benchmark, film resistance measurements were carried out. Samples were prepared by combining 100 μL of each PEDOT:dPSS product with a variable volume of DMSO (between 0 and 7.5 μL), and the solution was then spin-coated (18 s at minimum speed, then 60 s at 4000 rpm) on a poly(ethylene terephthalate) (PET) sheet and immediately then placed in oven for 5 min at 90 °C. After that, silver electrodes were drawn onto the sample, in the shape of squares, by using silver paste. The PET sheets were then replaced in the oven for 30 min at 90 °C. The resistance was then measured and compared to the benchmark. Light transmittance of the films was also measured by placing the PEDOT:dPSS-coated PET sheets in a spectrophotometer, with the incident wavelength = 550 nm. The reference sample was a plastic sheet which had not been spin-coated.

Sample Formulation. The dynamic light scattering (DLS) samples for aqueous EMIM:TCB solutions were prepared with concentrations between 0.1 and 3.5 mass % in two ways: (1) the water alone was filtered through a 0.2 μm syringe tip filter, and the EMIM:TCB was added straight to the sample, or (2) the EMIM:TCB was added to the water, and then the entire sample was filtered in the same fashion. The DLS samples for PEDOT:PSS were prepared by diluting the stock PH1000 solution 5000× to achieve a concentration of $\sim 2 \times 10^{-4}$ mass %, well within the dilute regime. The samples were then run through a 0.45 μm syringe tip filter into a cleaned glass vial and capped for measurement.

For small-angle neutron scattering (SANS), PEDOT:PSS/EMIM:TCB solutions were prepared by combining the ionic liquid directly into the vial containing the PH1000 (at stock concentration), and vortexing for >30 s. These solutions were then added to the appropriate sample cells for characterization. For contrast matching SANS experiments, the H_2O/D_2O solvent switching was carried out using pressure filtration under stirring (Millipore Amicon) with a 10 kDa cutoff filter. Specifically, the filtration cell was charged with 10 mL of PEDOT:PSS/PEDOT:dPSS and pressurized with N_2, magnetically stirred, and the total cell volume was monitored. Once the volume reached 2 mL, D_2O was back-added to the cell to increase the D_2O concentration to 80%. This process was repeated a minimum of four times to achieve a PEDOT:PSS solution with ≥99.8% D_2O concentration.

DOI: 10.1021/acs.macromol.5b02320
Macromolecules 2015, 48, 8989−8997

Characterization. Dynamic light scattering (DLS) measurements were performed on a BI-9000AT Brookhaven spectrometer (incident wavelength 488 nm). Molecular size was determined by analyzing the time autocorrelation, $g_2(\tau)$, defined as $g_2(\tau)) = \langle I(t)I(t+\tau)\rangle/\langle I(t)\rangle^2$, where $I(t)$ and $I(t+\tau)$ are the scattered intensities at some initial time t and some later time $t+\tau$ where τ is the delay time. The fluctuation correlation of light scattered from the particles will exponentially decay due to molecules undergoing longer range motion at long times. Polydispersity was taken into account by fitting the time autocorrelation function with an exponential decay function integrated over the relaxation rate distribution $G(\Gamma)$

$$g_2(\tau) = 1 + \beta' g_1^{\,2}(\tau), \quad g_1(\tau) = \int G(\Gamma)\exp(-\Gamma\tau)\,d\Gamma \qquad (1)$$

where $\Gamma = q^2D$, $q = (4\pi n_0/\lambda)\sin(\Theta/2)$, D is the diffusion coefficient, n_0 is the refractive index of the solvent, λ is the laser wavelength, and Θ is the scattering angle. From this, a size (R_h) was obtained through the Stokes–Einstein relationship, $D = k_BT/6\pi\eta_0R_h$, where T is the solution temperature, k_B is Boltzmann's constant, and η_0 is the solvent viscosity. For this work, a bimodal log-normal size distribution of particle aggregates was assumed for the data fitting.[42] For certain samples, multiangle DLS was carried out from $45° \le \Theta \le 115°$, and D was arrived at through plotting Γ vs q^2 and measuring the slope of the linear fit of the data. From there, the Stokes–Einstein relationship was also used to calculate R_h. Small-angle X-ray scattering (SAXS) experiments were carried out at the Laboratory for the Structure of Matter (LRSM) at the University of Pennsylvania on a Nonius FR591, which consists of a rotating anode generator operated at 40 kV × 85 mA, mirror–monochromator focusing optics, an evacuated flight path, and a Bruker HiSTAR multiwire two-dimensional detector. Data were collected at ~1 h intervals at a sample–detector distance of 11 cm. Small-angle neutron scattering (SANS) experiments were performed at the NIST Center for Neutron Research in Gaithersburg, MD, on the NGB 10 m SANS and the NG3 30 m SANS beamlines. On the 1 m SANS the sample-to-detector distance was adjusted between 1.1 and 5.3 m, and the wavelength was varied between 5 and 16 Å in order to measure scattering over a q-range of 0.003–0.5 Å^{-1}. Similarly, on the 30 m SANS the sample-to-detector distance was adjusted between 1.3 and 13.2 m at wavelengths of 6 and 8.4 Å in order to measure scattering over a q-range from 0.001 to 0.3 Å^{-1}.[43] For all SANS raw data or model fits, the statistical certainty was 1 standard deviation.

RESULTS AND DISCUSSION

EMIM:TCB in H_2O. As ionic liquids have been reported to have interesting behavior in various solvents, it was first key to understand the native structure of EMIM:TCB in water, as this would potentially effect the nature of the interaction with PEDOT:PSS in solution. In this context, EMIM:TCB aqueous solutions were studied with SAXS, DLS, and SANS. Figure 2 shows the SAXS data of neat EMIM:TCB, displaying a strong peak at $q = 1.23$ Å^{-1} ($d \sim 0.51$ nm) which is a common signature for neat ionic liquids, attributed to the ion-pair distance between the cation and anion of EMIM:TCB.[24]

When EMIM:TCB is diluted in water and analyzed in DLS, it displays strong ion-pair bonding behavior rather than exhibiting complete ion dissociation. This can be seen in Figure 3, which shows that EMIM:TCB in water exhibits a strong pair–pair correlation signal, representative of ionic liquid-rich droplet phases with diameters ~120–1000 nm. It is important to note that the upper bound of the size distribution of these ionic liquid-rich droplets is pseudoquantitative, as the correlation plot in Figure 3a does not reach a baseline, which indicates that larger scale, inhomegenous structures exist that have not relaxed within the time scale of the experiments. This is further underscored by time-dependent DLS experiments, in which the ionic liquid droplet population size exhibited a dynamic, ripening-like behavior where the size population shifted to larger droplet sizes as a function of time (data not shown). When these aqueous EMIM:TCB solutions are filtered through a 0.2 μm filter, there is a marked decrease in signal in DLS spectra coupled with a faster decay times compared to the unfiltered sample, providing evidence of the ability to physically remove these EMIM:TCB-rich liquid domains. It is important to note that these ionic liquid domains have been observed at concentrations between 0.1 and 3.5 mass % and can be physically filtered away using syringe tip filters for the entire concentration range (data not shown). The inset of Figure 3 shows SANS data of EMIM:TCB in water (and D_2O) from 0.2 to 5.0%, which has a clear q^{-4} Porod behavior, indicative of interfacial scattering from the smooth surface of a large ionic liquid droplet. In order to confirm these experimental results, analytical calculation of the ion-dissociation energy of EMIM:TCB in water was done and was found to be ~50k_BT. This large binding energy of the individual ions of EMIM:TCB in water corroborates the experimental observations.

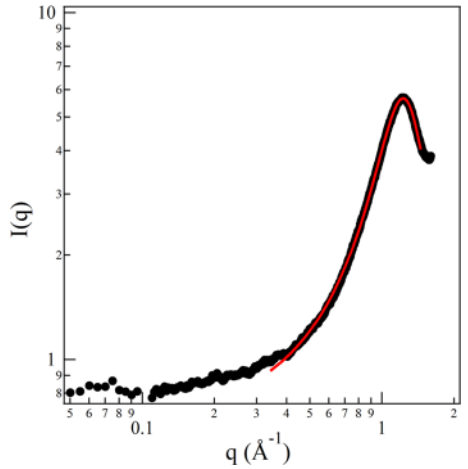

Figure 2. SAXS results for neat EMIM TCB. A Lorenzian peak curve fit (in red) identifies a clear peak at $q \sim 1.23$ Å^{-1} ($d \sim 5.1$ Å), which is attributed to the ion-pair peak between the EMIM cation and TCB anion.

PEDOT:PSS in H_2O. In order to understand the equilibrium solution structure of PEDOT:PSS, multiangle DLS was carried out on PEDOT:PSS, with the results shown in Figure 4. The linear regression fit of Γ vs q^2 gives a slope of $D \sim 1.389$ μm/s (R^2 of 0.9932) which gives an $R_h = 176$ nm. As described above, this sample was filtered through a 200 nm syringe tip filter before being measured. Thus, the data in Figure 4 confirm that the native structure of PEDOT:PSS is a microgel particle morphology with average diameters ≥300 nm rather than the tens of nanometer sized structures that have been previously reported.[9] The results in Figure 4 are in good agreement with recent electron microscopy results.[44] Although there is no direct evidence presented here, the good solution stability of PEDOT:PSS is likely driven by the microgels possessing a higher concentration of negatively charged PSS monomers at their exterior, which promotes electrostatic repulsion between microgels and prevents their aggregation.

The morphology of the interior of these microgels was investigated through SANS, and Figure 5 shows the results for 1.1 mass % PEDOT:PSS in >98% D_2O. In order to gain a better physical insight, the data were fit with the Broad Peak Model, which is an empirical model often used to fit neutral and charged polymer systems that exhibit electrostatically driven correlation behavior.[45] The model is defined as

DOI: 10.1021/acs.macromol.5b02320
Macromolecules 2015, 48, 8989–8997

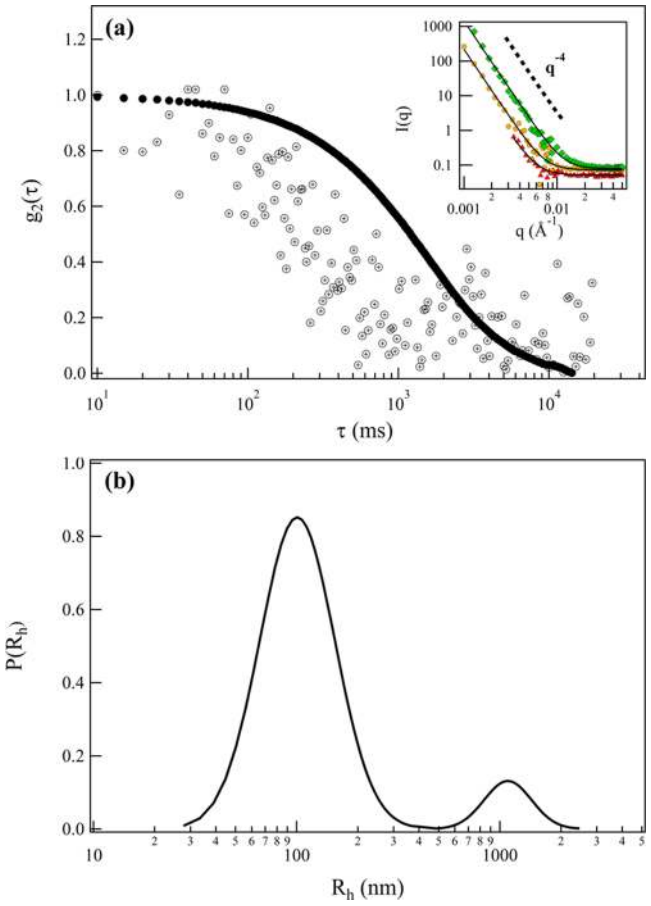

Figure 3. (a) DLS results (Θ = 90°) for 3.0 mass % EMIM TCB in water both (●) unfiltered and (⊕) filtered through a 0.2 μm syringe tip filter. Note: in both samples, the water used to make the samples was always filtered first, in order to eliminate scattering from solvent impurities. The unfiltered data were fit with a CONTIN-based, two relaxation mode exponential function, resulting in a bimodal distribution of EMIM TCB liquid droplets; $R_1 \sim 120$ nm and $R_2 \sim 1000$ nm. The filtered data were too noisy to fit confidently. Similar behavior of EMIM TCB in water was observed in DLS down to [EMIM TCB] ~ 0.001 mass %. Inset shows SANS results of (red △) 0.2%, (orange ○) 3.0%, and (green ◇) 5.0% EMIM TCB in D_2O. The solid lines are Porod model fits, showing a clear $I(q) \sim q^{-4}$ dependence which is characteristic of a sharp water−EMIM TCB interface. (b) Log-normal probability distributions of the bimodal size distribution of EMIM:TCB droplets in water.

$$I(q) = \frac{A}{q^n} + \frac{C}{1 + (|q - q_{max}|L)^m} + B \quad (2)$$

where n is the low-q scaling exponent, q_{max} is the interchain correlation peak position, L is the electrostatic screening length of the interchain correlation, m is the high-q scaling exponent, and B is the background incoherent scattering. The fitting results are shown in Table 1 of the Supporting Information. It is important to note here that the exponents n and m in eq 2 are inversely related to the well-known Flory exponent (ν) for polymer systems, i.e., n; $m \sim 1/\nu$. This scaling relationship provides the ability to determine chain conformation based on scaling behavior in a given solution over a particular range of length scales. In this context, the value of $n = -2.8$ in Figure 5 is indicative of a fairly condensed, uniformly entangled polymer mesh at 42 nm ≤ d ≤ 400 nm while the scaling of $m \sim 1.15$ indicates the chains are fairly rigid at $d \leq 10$ nm. The peak

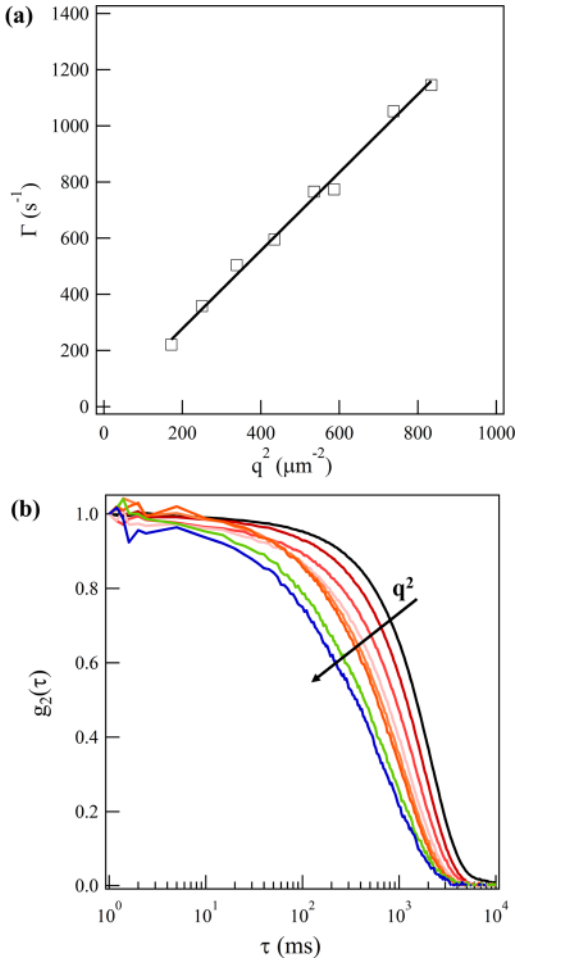

Figure 4. Multiangle dynamic light scattering results for a 2×10^{-4} mass % solution of PEDOT:PSS. (a) The Γ vs q^2 has a slope of $D \sim 1.389$ μm/s (R^2 of 0.9932), showing a microgel particle morphology with $R_h \approx 176$ nm. (b) Time correlation data as a function of increasing angle. To maintain a high purity sample, the solution was filtered through a 0.45 μm syringe tip filter; thus, there are likely much larger microgel particles in the native PEDOT:PSS solution.

value $q_{max} \sim 0.033$ Å denotes that PEDOT:PSS exhibits a lightly screened structural correlation at $d \sim 19$ nm with an electrostatic correlation length of $L = \sim 4.1$ nm.

As PEDOT:PSS is a polyelectrolyte, a serial dilution SANS study of PEDOT:PSS was conducted in order to investigate whether the q_{max} in Figure 5 is the well-known polyelectrolyte peak, which is caused by local rod-like structure along the chains derived from the like-charge repulsion of the highly charged backbone.[46] This distribution of rigid segments results in an interchain correlation peak in neutron, X-ray, and light scattering experiments with various polyelectrolyte systems.[47−55] The results of the dilution experiments shown in Figure 5 shows a $\xi \sim c^{-1/2}$, which is in strong agreement with the de Gennes theory denoting that on the $d \leq 300$ nm length scale the native structure of PEDOT:PSS inside the microgel is similar to a classic polyelectrolyte system in the semidilute regime. It is important to note that the larger values of ξ for PEDOT:PSS versus NaPSS (Figure 5) could be attributed to either the increased overall stiffness of PEDOT:PSS due to the presence of PEDOT oligomers complexed along the PSS backbone chain or the increased finite chain thickness of PEDOT:PSS when compared to PSS only. The combination of

DOI: 10.1021/acs.macromol.5b02320
Macromolecules 2015, 48, 8989−8997

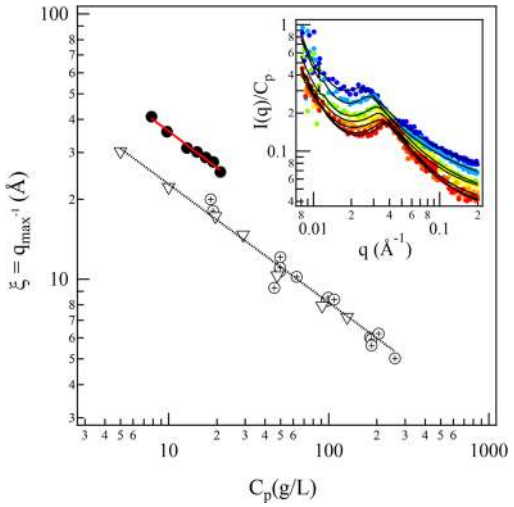

Figure 5. Dilution SANS measurements comparing ξ between PEDOT:PSS (●) and NaPSS from PSS from ref 47 (▽) and from ref 55 (⊕) showing the characteristic shift of ξ (= q_{max}^{-1}) with polyelectrolyte concentration (C_p). Data from refs 47 and 55 used with permission. All data were fit with the power law $f(x) = Ax^n$. The red line represents a fit with $n = -0.455 \pm 0.022$ and $A = 102.85$, while the dashed black line has $n = -0.504 \pm 0.01$ and $A = 81.23$. These fitting results confirm the polyelectrolyte scaling behavior of $\xi \sim C_p^{-1/2}$ for PEDOT:PSS. The increase in A denotes a larger average ξ for PEDOT:PSS compared to PSS alone, which illustrates the increased chain stiffness from the conjugated PEDOT oligomers along the PSS backbone. Inset shows the dilution series raw data, $I(q)/C_p$ vs q, fit with the model shown in eq 2.

Figures 4 and 5 results in a novel, multilength scale structural model of native PEDOT:PSS that to our knowledge has yet to be proposed in the literature (see Figure 10).

PEDOT:PSS + EMIM:TCB. Upon addition of EMIM:TCB to PEDOT:PSS, the SANS data shown in Figure 6 signify a distinct change in the native PEDOT:PSS structure that results in a disruption the polyelectrolyte interchain correlation, q_{max}. In order to quantify the change in PEDOT:PSS structure with the addition of EMIM:TCB, the curves in Figure 6 were fit with eq 2, and the fitting results are shown in Table 1 of the Supporting Information.

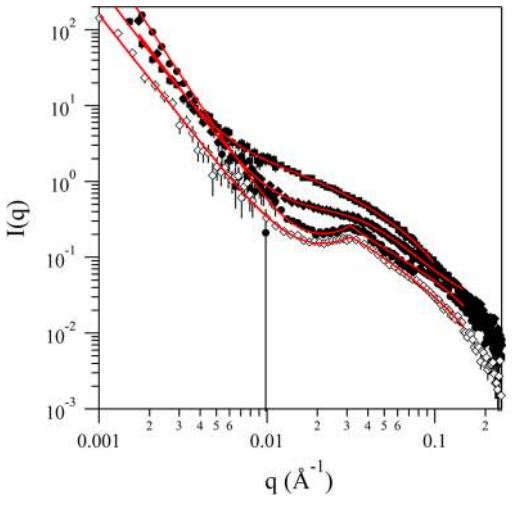

Figure 6. SANS results for PEDOT:PSS with (◇) 0.0, (●) 0.015, (◆) 0.4, and (■) 1.5 mass % EMIM TCB. Red lines represent the fits of eq 2 for each EMIM:TCB concentration. The 0.0% EMIM:TCB data and model fit here is reproduced from Figure 5.

First, it is clear that the PEDOT:PSS is increasingly neutralized as EMIM:TCB concentration is increased. Given the anionic nature of the PSS, this structural change of PEDOT:PSS is likely driven by the association of the EMIM cation to the PSS backbone. This conjecture can be rationalized by the fact that as EMIM:TCB concentration is increased, q_{max} systematically decreases, which represents an increase in the distance between charged, locally rigid segments of the polyelectrolyte chain. Along with the decrease of q_{max}, the correlation length between neutral chain segments, L, decreases as EMIM:TCB concentration increases, which is an expected observation when interchain charge repulsion is screened. It is also clear from Table 1 (Supporting Information) that the high-q slope (n) increases from ∼1 to ∼1.66, which from eq 2 is indicative of transition from a more rigid to a more coil-like chain structure at short length scales. It is important to note that at the highest concentration of EMIM:TCB measured (1.5%) L is not an applicable parameter due to q_{max} having decreased to a negligible value at this condition.

The conjecture of the specific interaction of EMIM:TCB with PEDOT:PSS was directly tested through contrast matching SANS experiments, and the results are shown in Figure 7. In these tests, the contrast match point for deuterated PSS (dPSS) was directly measured by systematically varying the H_2O/D_2O solvent ratio for a solution of dPSS and finding the condition in which there was no scattering above the solvent background for all scattering angles. These experiments yielded

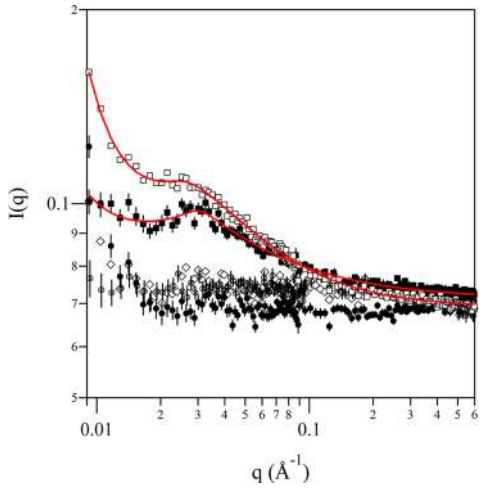

Figure 7. Contrast matching SANS of dPSS with (●) 0.0%, (◇) 0.25%, (■) 0.5%, and (□) 0.7% EMIM:TCB. For comparison, (⊕) is 5.0% DMSO. The 0.5% and 0.7% EMIM:TCB samples were fit with eq 2 for comparison. A clear recovery of the dPSS structure is observed as [EMIM:TCB] is increased. The recovery of the polyelectrolyte peak at EMIM:TCB = 0.5 mass % (q = 0.030 Å) denotes an incomplete chain complexation between the EMIM cation and the dPSS chain. As EMIM:TCB = 0.7 mass %, the slight shift of the polyelectrolyte peak to lower q (q = 0.026 Å) and the broadening of the peak width denotes a larger degree of neutralization of the dPSS due to a higher degree of EMIM cation complexation. Interestingly, the DMSO sample looks very similar to the PEDOT:PSS only curve, which points to a strong difference in interaction between PEDOT:PSS and DMSO compared to EMIM:TCB. Note that the contrast match point for dPSS is 100% D_2O and that each curve has been normalized by their background value in order to visualize the data clearly.

DOI: 10.1021/acs.macromol.5b02320
Macromolecules 2015, 48, 8989−8997

a contrast match point of 100% D_2O for dPSS. A series of 1.0 mass % dPSS solutions in 100% D_2O were then prepared at various EMIM:TCB concentrations and measured to observe any deviation in the scattering signature above background. In Figure 7, there is very little change in the data relative to the control sample for the lowest EMIM:TCB concentration. Interestingly, as the EMIM:TCB concentration is further increased, as a scattering signature typical for polyelectrolytes is observed, as evidenced by the emergence of a $q_{max} \sim 0.03$ Å^{-1}. Upon further addition of EMIM:TCB, the data are indicative of a more neutral polyelectrolyte system, as peak broadens significantly, and the q_{max} appears to shift to lower q values. The 0.5% and 0.7% EMIM:TCB samples were fit with eq 2, and the complete fitting results are shown in Table 2 of the Supporting Information. We argue that the behavior in Figure 7 is direct evidence of the EMIM cation association to the dPSS chain. In this system, if the EMIM:TCB ion pair was disrupted, the EMIM cation would tend to associate with the negatively charged pendant groups of the dPSS chain due to electrostatic attraction and thereby disrupt the contrast match condition of the pure dPSS sample. This change in the contrast match point of the dPSS due to the association with EMIM cations results in a recovery in the various scattering signatures of the pure dPSS as [EMIM:TCB] increases, i.e., polyelectrolyte peak at low [EMIM:TCB] and more neutral polymer behavior at high [EMIM:TCB]. The fitting results in Table 2 (Supporting Information) corroborate this conjecture.

In order to further test the conjecture of EMIM-cation/PSS interaction, PEDOT:deuterated-PSS (PEDOT:dPSS) was synthesized and measured in SANS at the contrast match point of dPSS at various concentrations of EMIM:TCB. Under these conditions, the scattering pattern should only be representative of the PEDOT oligomers or dPSS chain segments that are complexed with EMIM cations. The results are shown in Figure 8.

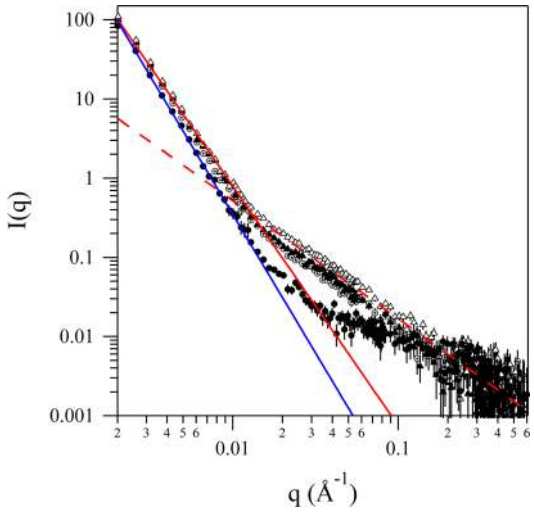

Figure 8. Contrast match experiments of PEDOT:dPSS at 100% D_2O with (●) 0.0%, (⊕) 0.25%, (▲) 0.4%, and (△) 0.7% EMIM:TCB. The solid and dashed red lines are power law plots for the PEDOT:dPSS + EMIM:TCB samples and have slope values of −3.0 and −1.50, respectively. The blue line is a power law fit for the low q region of the pure PEDOT:dPSS sample and has a slope of −3.5. This difference between the low q slopes of PEDOT:dPSS with and without EMIM:TCB points to a slight decrease in the PEDOT network density upon addition of EMIM:TCB.

For all of the samples measured, there is a dramatic difference in the scattering profiles at this contrast matched condition compared to the noncontrast matched samples shown in Figure 6. For the pure PEDOT:PSS case, the low q slope value increases slightly ($n = -3.5$ compared to −3.06), and there is only slight evidence of the q_{max} peak at $q \sim 0.02$ Å^{-1}. The low q slope value of $n = -3.5$ is likely attributed to the fact that at the contrast matching of the flexible dPSS polymer, the PEDOT oligomer network scatters more like a fairly dense, branched network of rigid units[56] rather than the mass fractal scattering behavior of a polymer mesh. An illustration of this conjecture is shown in Figure 10c. Although quite small, the evidence of the polyelectrolyte peak at $q \sim 0.02$ Å is likely due to slight deviations between the theoretical contrast match point for 100% sulfonated PSS and what was experimentally determined for ≥83% PSS. This incomplete sulfonation is likely promoting a slight contribution of the dPSS structure to the scattering signature.

As EMIM:TCB is added, the low q slope reverts back to $n = -3.0$, and at $q \sim 0.015$ Å^{-1} there is a clear slope change to $n = -1.50$ that persists for over an order of magnitude in q. The change in value of n of these samples corroborates the results from Figure 7; the EMIM cation/PSS backbone interaction changes the scattering length density of the PSS resulting in scattering behavior indicative of a polymer mesh, similar to what is observed in Figure 5a for commercial PEDOT:PSS in water. Furthermore, we argue that this slope change for $q \geq 0.015$ Å^{-1} is further evidence of the EMIM cation complexation onto dPSS. Taking the scaling relationship described above into account ($I(q) \sim q^{-d_f}$; $d_f \sim 1/\nu$), the samples with added EMIM:TCB in Figure 8 at $q \geq 0.015$ Å^{-1} have a value of $\nu \sim 0.66$, which is indicative of the dPSS taking on the behavior of a semiflexble polymer in good solvent at a length scale of ≤42 nm (Figure 10d). This good solvent scaling in polyelectrolyte systems is a signature of neutralization via ion complexation, which in this system must be driven by EMIM cation complexation with the dPSS chain. This result is in very good agreement with the fitting results in Table 1 (Supporting Information) for 0.4 and 1.5 mass % EMIM:TCB, which have scaling exponents that denote the local chain structure shifting from a stiff to a more flexible conformation as EMIM:TCB is added.

It is important to note that although the exact nature of the EMIM cation/PSS interaction at the molecular level is not fully understood, the interaction between these two species is unique when compared to standard salts such as NaCl. Comparison studies were done by adding various concentrations of NaCl to PEDOT:PSS, which resulted in macroscopic flocculation above a critical concentration (data not shown).

PEDOT:PSS + DMSO. In order to compare the effect of EMIM:TCB and DMSO (a widely reported performance enhancing additive) on the PEDOT:PSS structure, Figure 9 shows the SANS data of PEDOT:PSS in solution as a function of DMSO concentration. Note that all curves in Figure 9 are fit with eq 2, and the results are shown Table 3 of the Supporting Information. This data are in stark contrast to Figure 6, as the overall structure of PEDOT:PSS is relatively independent of DMSO concentration. It is important to note that the q_{max} position of the polyelectrolyte peak does shifts slightly to lower q, as DMSO concentration up to 15 mass %. However, this shift in q_{max} is far less dramatic than that shown in Figure 6, which points to only a slight electrostatic screening of the PEDOT:PSS chain by DMSO compared to that by

DOI: 10.1021/acs.macromol.5b02320
Macromolecules 2015, 48, 8989−8997

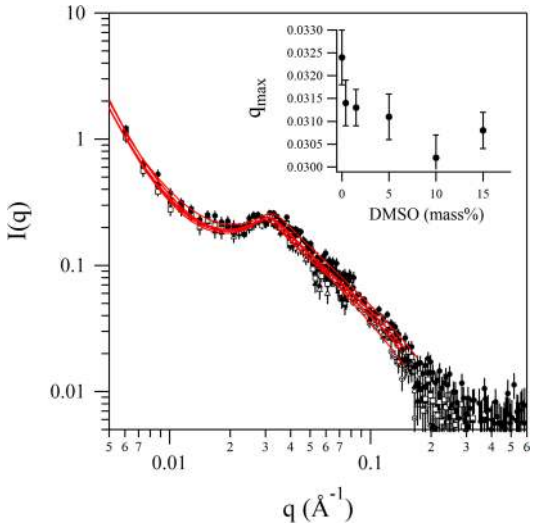

Figure 9. SANS results for PEDOT:PSS (●) 0.0, (⊕) 0.4, (■) 1.5, (□) 5.0, (▲) 10.0, and (△) 15.0 mass % DMSO. Each curve is fit with eq 2, and the fit results are shown in Table 2 of the Supporting Information. The inset shows a slight shift of the polyelectrolyte peak to lower q as DMSO increases; however, the overall structure of PEDOT:PSS largely independent of DMSO concentration.

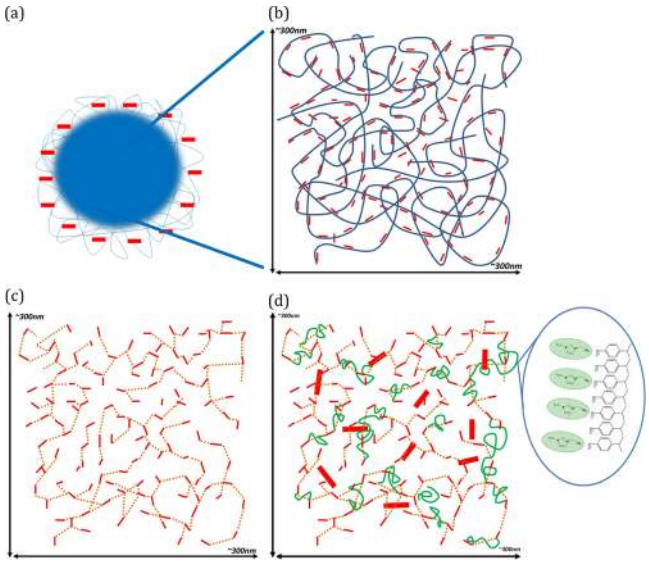

Figure 10. Illustration summarizing the multilength scale structural model of PEDOT:PSS with EMIM:TCB. (a) At length scales ≥300 nm, the pure PEDOT:PSS solution is a dispersion of electrostatically stabilized microgels. (b) The interior of these microgels is an entangled polyelectrolyte mesh of relatively stiff individual PEDOT:PSS chains, where the blue chains represent the PSS and the red represents PEDOT. (c) How the PEDOT:dPSS structure appears under the dPSS contrast match conditions, giving rise to a scaling relationship of a branched network structure. (d) Interaction of the EMIM cation with dPSS in the contrast matched condition gives rise to two discrete scaling behaviors in SANS; a compact chain mesh at larger length scales and a semiflexible swollen chain at smaller length scales.

EMIM:TCB. The independance of the PEDOT:PSS structure to DMSO is underscored by the dPSS contrast match experiment (Figure 7), as the addition of DMSO to dPSS does not notably change the scattering profile when compared to the dPSS alone. These two results clearly point to a wholly different mechanism between EMIM:TCB and DMSO in the solution state; the EMIM:TCB interacts with the PEDOT:PSS via electrostatic interactions and alters its overall structure, while the DMSO appears to not interact with the interior of the PEDOT:PSS microgel while in solution.

CONCLUSION

Through a combination of SAXS and SANS, a novel structural model for PEDOT:PSS has been presented that describes the system from the ∼1 μm to ∼1 nm length scale and is illustrated in Figure 10. The native PEDOT:PSS exhibits a loose microgel structure at length scales $d \geq 300$ nm, which are likely electrostatically stabilized by PSS chain segments not complexed with PEDOT oligomers. The interior of these microgels has an entangled mesh architecture similar to classic polyelectrolyte systems in the semidilute regime. The addition of EMIM:TCB to the PEDOT:PSS dispersion causes a dissociation of the strong ion-pairing between the EMIM cation and TCB anion, resulting in EMIM cation complexation with the PSS backbone causing neutralization of the PSS and a unique change in the polymer network structure.

Finally, although illustrated in Figure 10, there is no direct experimental evidence herein that shows dissociation of the PEDOT oligomers away from the PSS chains as EMIM:TCB is added. It is conjectured that this is a likely consequence of the EMIM cation/PSS chain interaction described above, and future research will focus on understanding the nature of the PEDOT oligomers as a function of EMIM:TCB concentration. Inspired by recent grazing incidence studies on PEDOT:PSS,[10,35] current studies are underway focusing on understanding the discrete interaction behaviors between PEDOT:PSS and other ionic liquids and simple salt systems, as well as if these solution structures have any effect on the film structure and conductivity performance.

ASSOCIATED CONTENT

Supporting Information

The Supporting Information is available free of charge on the ACS Publications website at DOI: 10.1021/acs.macromol.5b02320.

Fitting results for all Broad Peak Model curve fits (PDF)

AUTHOR INFORMATION

Corresponding Author

*E-mail: ryan.murphy@solvay.com (R.J.M.).

Funding

This manuscript has been authored by UT-Battelle, LLC under Contract DE-AC05-00OR22725 with the U.S. Department of Energy. The United States Government retains and the publisher, by accepting the article for publication, acknowledges that the United States Government retains a nonexclusive, paid-up, irrevocable, worldwide license to publish or reproduce the published form of this manuscript, or allow others to do so, for United States Government purposes. The Department of Energy will provide public access to these results of federally sponsored research in accordance with the DOE Public Access Plan (http://energy.gov/downloads/doe-public-access-plan).

Notes

The authors declare no competing financial interest.

DOI: 10.1021/acs.macromol.5b02320
Macromolecules 2015, 48, 8989−8997

■ ACKNOWLEDGMENTS

We thank Solvay for the majority funding of this research. A portion of this research was conducted through project 2013-263 at the Center for Nanophase Materials Sciences, which is sponsored at Oak Ridge National Laboratory by the Scientific User Facilities Division, Office of Basic Energy Sciences, U.S. Department of Energy. We also acknowledge the support of the National Institute of Standards and Technology, U.S. Department of Commerce, in providing the neutron research facilities used in this work. R.J.M. thanks Peter Bonnesen at the CNMS for his assistance on the synthesis of deuterated PEDOT:PSS, Boualem Hammouda at the NIST Center for Neutron Research for technical discussions, Paul Heiney at the University of Pennsylvania for his assistance in SAXS measurements, and Ron Jones at the nSoft Industrial Neutron Consortium at NIST for support in facilitating the neutron experiments. M.M. acknowledges the support from the National Science Foundation Grant DMR-1504265.

■ ADDITIONAL NOTE

[a]Certain commercial equipment, instruments, or materials are identified in this paper in order to specify the experimental procedure adequately. Such identification is not intended to imply recommendation or endorsement by the National Institute of Standards and Technology, nor is it intended to imply that the materials or equipment identified are necessarily the best available for the purpose.

■ REFERENCES

(1) Roncali, J. *Chem. Rev.* **1992**, *92*, 711−738.
(2) Elschner, A.; Krichmeyer, S.; Lovenich, W.; Merker, U.; Reuter, K. *PEDOT - Principles and Applications of an Intrinsically Conductive Polymer*; CRC Press: Boca Raton, FL, 2011.
(3) Scott, J. C.; Malliaras, G. G.; Chen, W. D.; Breach, J. C.; Salem, J. R.; Brock, P. J.; Sachs, S. B.; Chidsey, C. E. D. *Appl. Phys. Lett.* **1999**, *74*, 1510−1512.
(4) Kim, J. Y.; Jung, J. H.; Lee, D. E.; Joo, J. *Synth. Met.* **2002**, *126*, 311−316.
(5) Bagchi, D.; Menon, R. *Chem. Phys. Lett.* **2006**, *425*, 114−117.
(6) Wilson, P.; Lekakou, C.; Watts, J. F. *Org. Electron.* **2013**, *14*, 3277−3285.
(7) Crispin, X.; Marciniak, S.; Osikowicz, W.; Zotti, G.; Van der Gon, A. W. D.; Louwet, F.; Fahlman, M.; Groenendaal, L.; De Schryver, F.; Salaneck, W. R. *J. Polym. Sci., Part B: Polym. Phys.* **2003**, *41*, 2561−2583.
(8) Crispin, X.; Jakobsson, F. L. E.; Crispin, A.; Grim, P. C. M.; Andersson, P.; Volodin, A.; van Haesendonck, C.; Van der Auweraer, M.; Salaneck, W. R.; Berggren, M. *Chem. Mater.* **2006**, *18*, 4354−4360.
(9) Takano, T.; Masunaga, H.; Fujiwara, A.; Okuzaki, H.; Sasaki, T. *Macromolecules* **2012**, *45*, 3859−3865.
(10) Palumbiny, C. M.; Heller, C.; Schaffer, C. J.; Korstgens, V.; Santoro, G.; Roth, S. V.; Muller-Buschbaum, P. *J. Phys. Chem. C* **2014**, *118*, 13598−13606.
(11) Alemu, D.; Wei, H. Y.; Ho, K. C.; Chu, C. W. *Energy Environ. Sci.* **2012**, *5*, 9662−9671.
(12) Xia, Y. J.; Ouyang, J. Y. *Macromolecules* **2009**, *42*, 4141−4147.
(13) Fan, B. H.; Mei, X. G.; Ouyang, J. Y. *Macromolecules* **2008**, *41*, 5971−5973.
(14) Dobbelin, M.; Marcilla, R.; Salsamendi, M.; Pozo-Gonzalo, C.; Carrasco, P. M.; Pomposo, J. A.; Mecerreyes, D. *Chem. Mater.* **2007**, *19*, 2147−2149.
(15) Dobbelin, M.; Marcilla, R.; Tollan, C.; Pomposo, J. A.; Sarasua, J. R.; Mecerreyes, D. *J. Mater. Chem.* **2008**, *18*, 5354−5358.
(16) Dobbelin, M.; Tena-Zaera, R.; Marcilla, R.; Iturri, J.; Moya, S.; Pomposo, J. A.; Mecerreyes, D. *Adv. Funct. Mater.* **2009**, *19*, 3326−3333.
(17) Dobbelin, M.; Marcilla, R.; Pozo-Gonzalo, C.; Mecerreyes, D. *J. Mater. Chem.* **2010**, *20*, 7613−7622.
(18) Markus Bier, S. D. arXiv 2009, cond-mat.matrl-sci2090v1.
(19) Lopes, J.; Padua, A. A. H. *J. Phys. Chem. B* **2006**, *110*, 3330−3335.
(20) Wang, Y. T.; Voth, G. A. *J. Phys. Chem. B* **2006**, *110*, 18601−18608.
(21) Jiang, W.; Wang, Y. T.; Voth, G. A. *J. Phys. Chem. B* **2007**, *111*, 4812−4818.
(22) Triolo, A.; Russina, O.; Bleif, H. J.; Di Cola, E. *J. Phys. Chem. B* **2007**, *111*, 4641−4644.
(23) Triolo, A.; Russina, O.; Fazio, B.; Triolo, R.; Di Cola, E. *Chem. Phys. Lett.* **2008**, *457*, 362−365.
(24) Triolo, A.; Russina, O.; Fazio, B.; Appetecchi, G. B.; Carewska, M.; Passerini, S. *J. Chem. Phys.* **2009**, *130*, 164521.
(25) Lipsztajn, M.; Osteryoung, R. A. *J. Electrochem. Soc.* **1983**, *130*, 1968−1969.
(26) McEwen, A. B.; Ngo, H. L.; LeCompte, K.; Goldman, J. L. *J. Electrochem. Soc.* **1999**, *146*, 1687−1695.
(27) Buzzeo, M. C.; Evans, R. G.; Compton, R. G. *ChemPhysChem* **2004**, *5*, 1106−1120.
(28) Fukaya, Y.; Sugimoto, A.; Ohno, H. *Biomacromolecules* **2006**, *7*, 3295−3297.
(29) Domanska, U.; Krolikowska, M.; Acree, W. E.; Baker, G. A. *J. Chem. Thermodyn.* **2011**, *43*, 1050−1057.
(30) Marciniak, A. *Int. J. Mol. Sci.* **2011**, *12*, 3553−3575.
(31) Viboud, S.; Papaiconomou, N.; Cortesi, A.; Chatel, G.; Draye, M.; Fontvieille, D. *J. Hazard. Mater.* **2012**, *215*, 40−48.
(32) Badre, C.; Marquant, L.; Alsayed, A. M.; Hough, L. A. *Adv. Funct. Mater.* **2012**, *22*, 2723−2727.
(33) Xia, Y. J.; Ouyang, J. Y. *ACS Appl. Mater. Interfaces* **2012**, *4*, 4131−4140.
(34) Wei, Q. S.; Mukaida, M.; Naitoh, Y.; Ishida, T. *Adv. Mater.* **2013**, *25*, 2831−2836.
(35) Palumbiny, C. M.; Liu, F.; Russell, T. P.; Hexemer, A.; Wang, C.; Muller-Buschbaum, P. *Adv. Mater.* **2015**, *27*, 3391−3397.
(36) Hsieh, H.; Quirk, R. *Anionic Polymerization: Principles and Practical Applications*; Marcel Dekker: New York, 1996.
(37) Hadjichristidis, N.; Iatrou, H.; Pispas, S.; Pitsikalis, M. *J. Polym. Sci., Part A: Polym. Chem.* **2000**, *38*, 3211−3234.
(38) Uhrig, D.; Mays, J. W. *J. Polym. Sci., Part A: Polym. Chem.* **2005**, *43*, 6179−6222.
(39) Valint, P. L.; Bock, J. *Macromolecules* **1988**, *21*, 175−179.
(40) Yang, J. C.; Mays, J. W. *Macromolecules* **2002**, *35*, 3433−3438.
(41) Louwet, F.; Groenendaal, L.; Dhaen, J.; Manca, J.; Van Luppen, J.; Verdonck, E.; Leenders, L. *Synth. Met.* **2003**, *135*, 115−117.
(42) Stepanek, P. *J. Chem. Phys.* **1993**, *99*, 6384−6393.
(43) Glinka, C. J.; Barker, J. G.; Hammouda, B.; Krueger, S.; Moyer, J. J.; Orts, W. J. *J. Appl. Crystallogr.* **1998**, *31*, 430−445.
(44) Gangopadhyay, R.; Das, B.; Molla, M. *RSC Adv.* **2014**, *4*, 43912−43920.
(45) Horkay, F.; Hammouda, B. *Colloid Polym. Sci.* **2008**, *286*, 611−620.
(46) Degennes, P. G.; Pincus, P.; Velasco, R. M.; Brochard, F. *J. Phys.* **1976**, *37*, 1461−1473.
(47) Nierlich, M.; Williams, C. E.; Boue, F.; Cotton, J. P.; Daoud, M.; Farnoux, B.; Jannink, G.; Picot, C.; Moan, M.; Wolff, C.; Rinaudo, M.; Gennes, P. G. D. *J. Phys.* **1979**, *40*, 701−704.
(48) Ise, N.; Okubo, T. *Acc. Chem. Res.* **1980**, *13*, 303−309.
(49) Ise, N.; Okubo, T.; Hiragi, Y.; Kawai, H.; Hashimoto, T.; Fujimura, M.; Nakajima, A.; Hayashi, H. *J. Am. Chem. Soc.* **1979**, *101*, 5836−5837.
(50) Ise, N.; Okubo, T.; Yamamoto, K.; Matsuoka, H.; Kawai, H.; Hashimoto, T.; Fujimura, M. *J. Chem. Phys.* **1983**, *78*, 541−545.
(51) Ise, N.; Okubo, T.; Kunugi, S.; Matsuoka, H.; Yamamoto, K.; Ishii, Y. *J. Chem. Phys.* **1984**, *81*, 3294−3306.
(52) Drifford, M.; Dalbiez, J. P. *J. Phys. Chem.* **1984**, *88*, 5368−5375.
(53) Nierlich, M.; Boue, F.; Lapp, A.; Oberthur, R. *Colloid Polym. Sci.* **1985**, *263*, 955−964.

DOI: 10.1021/acs.macromol.5b02320
Macromolecules 2015, 48, 8989−8997

(54) Borsali, R.; Nguyen, H.; Pecora, R. *Macromolecules* **1998**, *31*, 1548−1555.
(55) Prabhu, V. M.; Muthukumar, M.; Wignall, G. D.; Melnichenko, Y. B. *J. Chem. Phys.* **2003**, *119*, 4085−4098.
(56) Mehta, R.; Dadmun, M. D. *Macromolecules* **2006**, *39*, 8799−8807.

DOI: 10.1021/acs.macromol.5b02320
Macromolecules 2015, 48, 8989−8997